# Measurement of Internal Geometry of Small Surface Crack by Ultrasonic Method*
## (Relation between Back Reflection Intensity, Crack Depth and Crack Deflection)

Roziq HIMAWAN**, Yoshio ARAI**
and Eiichiro TSUCHIDA**

In this study, an ultrasonic technique for quantitative nondestructive evaluation of a small surface fatigue crack was developed. The use of an oblique longitudinal wave with large angle (over the critical angle) of incidence upon a specimen surface was emphasized. Ultrasonic testing was performed for a specimen with small surface fatigue cracks and artificial defects. We have used maximum amplitude of reflection echo due to these defects as a parameter, to evaluate them quantitatively. From such measurements, we have concluded that with the use of this parameter, surface fatigue cracks with more than 115 μm of surface length can be detected. Simultaneously, crack depth and deflection can also be detected. Based on these experimental results, we have proposed a set of experimental equations to evaluate the surface length and depth of crack. Finally, a model based on three-dimensional elastodynamics was proposed to simulate this ultrasonic technique, and numerical analysis was performed for the surface crack reflection problem.

***Key Words***: Nondestructive Inspection, Ultrasonic Inspection, Low Cycle Fatigue, Fatigue, Surface Crack, Reliability, Numerical Analysis, Notch

### 1. Introduction

It is known that the fatigue life of materials is controlled by the nucleation and propagation period of small surface cracks less than 1 mm in length[1]. To evaluate the fatigue life of a mechanical structure accurately, it is important to measure the geometry of a small surface crack (surface length, depth and deflection) nondestructively in the early stage of fatigue life. However, the minimum detectable crack size of the current ultrasonic technique is large, therefore, the remaining life after crack detection is short. On the other hand, many studies have been carried out with through cracks or artificial through notches. The depth measurement of fatigue cracks which propagated from artificial through cracks was performed using the ultrasonic water immersion method with perpendicular and small angle of incidence[2),(3)]. From interference fringe images of an ultrasonic microscope, the presence of surface cracks was detected and their depth measured[4]. Using surface waves generated from a contact transducer fixed on a specimen, a simultaneous measurement method of surface fatigue crack length and depth using a proof graph was proposed[5]. Consequently, to establish fatigue life management, it is important to develop a nondestructive evaluation method, which can minimize the minimum detectable size and measure the internal geometry of small surface fatigue cracks less than 1 mm in length nucleated from smooth specimens.

The aim of this study is to investigate the validity of the ultrasonic water immersion method with oblique incidence to evaluate low-cycle fatigue damage non-destructively. We proposed a method to evaluate both depth and deflection of small surface fatigue cracks using the change of maximum amplitude of reflected waves due to the change of the distance between the incidence point and cracks. After the measurement, the cross sections of cracks were observed and crack depth and deflection were

* Received 28th March, 2002. Japanese original: Trans. Jpn. Soc. Mech. Eng., Vol. 67, No. 655, A (2001), pp. 446-453 (Received 18th April, 2000)

** Saitama University, Department of Mechanical Engineering, 255 Shimo Ohkubo, Saitama, Saitama 338-8570, Japan. E-mail: yarai@mech.saitama-u.ac.jp

measured directly. An experiment using an artificial through notches of vaious depths was also conducted. Moreover, numerical analysis based on three-dimensional elastodynamics was conducted, and the results were compared to experimental ones. Finally, under the present experimental conditions, we proposed a set of experimental equations to evaluate the surface length and depth of cracks, and examined their validity.

## 2. Experimental Method

The material used was austenite stainless steel SUS304. Tables 1 and 2 show the chemical compositions and mechanical properties, respectively. Figure 1 shows the specimen shape and dimensions. Average grain diameter was measured using the method described in Ref.(6). The center portion of the specimen was fine polished using sand paper (#1500) and buff polishing. Ultrasonic measurement was conducted on two types of defects, namely small surface fatigue cracks and artificial notches (slits). Small surface fatigue cracks were introduced by subjecting the specimen to repeated loading using an electro-hydraulic material testing machine (MTS810). The loading was plane bending whose nominal bending stress was kept constant at 330 MPa, the stress ratio was $-1$, and loading frequency was 2 Hz. The environment was the atmosphere. Artificial notches were introduced by electro-discharge machining, and were 0.3 mm and 1.0 mm in width and length, respectively, and the notch depth varied from 70 to 314 μm.

Table 1 Chemical compositions [wt%]

| C | Si | Mn | P | S | Ni | Cr | Fe |
|---|---|---|---|---|---|---|---|
| 0.05 | 0.66 | 1.81 | 0.03 | 0.05 | 8.76 | 18.34 | Bal. |

Table 2 Mechanical properties

| E(GPa) | ν | $\sigma_{0.2}$(MPa) | $\sigma_{\beta}$(MPa) |
|---|---|---|---|
| 195.0 | 0.25 | 331.3 | 662.4 |

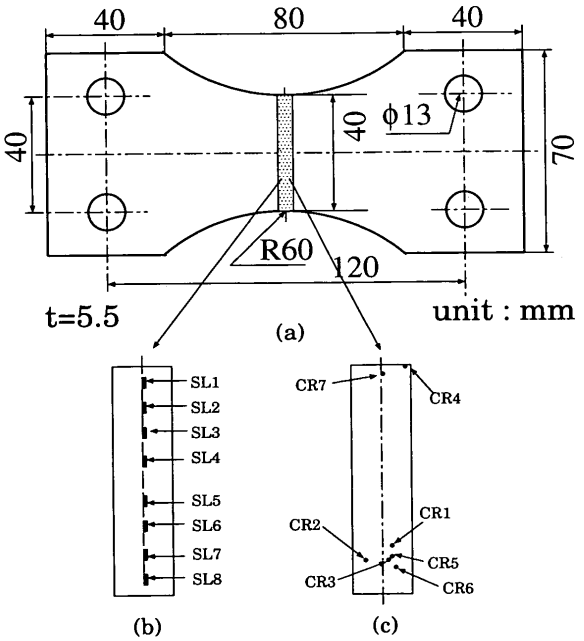


(a) Specimen geometry [unit: mm], (b) Location of slits, (c) Location of cracks

Fig. 1 Schematic of specimen

The center part of the specimen (±10 mm from center as illustrated in Fig. 1) was the observed area. Ultrasonic measurements were carried out using the immersion method as shown in Fig. 2. After subjecting the load of a prescribed cycle number (e.g. $N=$ 500, 1 500, 2 000), crack nucleation and propagation were observed under an optical microscope, and some images were captured. The crack lengths were measured as the projection length perpendicular to the loading direction. Reflected waves from the unloaded specimen surface were measured using a transducer which had the frequency of 10 MHz, incidence angle of 30°, focal distance of 25.4 mm in water, and beam diameter at focal point of about 1.0 mm. Ultrasonic waves generated from a pulsar were transmitted to the specimen surface. As the incidence angle is larger than the critical angle, it results in generation of surface waves which propagated through the surface. The surface waves were reflected by surface cracks. The leaky reflected surface waves were received at the incidence point by the same transducer. After the received signal was digitized by an A/D converter (sampling rate of 100 MHz), the data was acquired by a PC. The parameter used for evaluation was the maximum amplitude of reflected waves defined as $A$, as shown in Fig. 2.

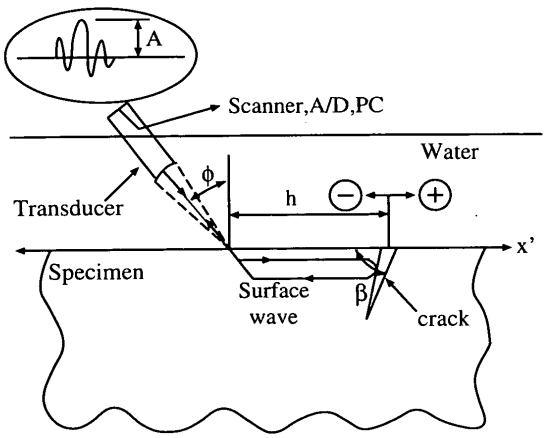


Fig. 2 Diagram of immersion ultrasonic for crack detection system

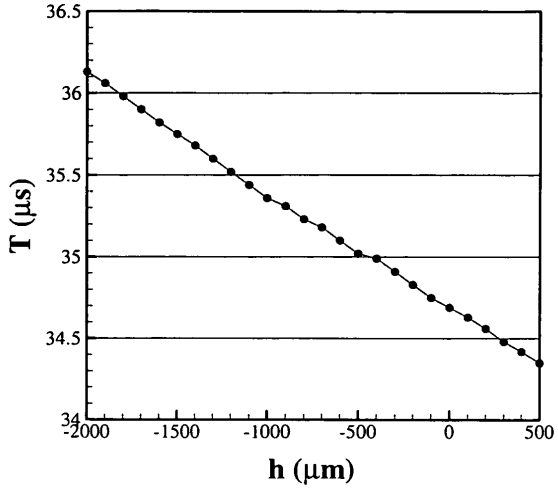


Fig. 3 Relationship between transmission and distance

Figure 3 shows the relationship between ultrasonic wave traveling time $T$ and incidence position $h$. From the slope in this figure, the velocity of the ultrasonic surface waves was calculated (2 830 m/s). The calculation result from material constants was 2 860 m/s. These two results are quite close. Therefore, it was confirmed that the received waves were leaky reflected surface waves. As the relative distance between incidence positions and cracks (or artificial notches) change, the value of $A$ changes. When $A$ takes a maximum value, it is defined as $A_{max}$, and the incidence position $h$, is defined as zero ($h=0$). Each defect was scanned in the $x'$-direction $\pm 2$ mm from the origin, (crack position) with a 100 μm incremental step. At each step, the waveform was acquired. In order to examine the crack deflection in the depth, incidence angle $\phi$ was changed to $-30°$, and the same procedure of measurements was conducted. After ultrasonic measurement, the specimen was cut and polished to observe the crack crosssection and measure the depth of crack.

### 3. Ultrasonic Evaluation Model

As shown in Fig. 4, the transducer was modeled as a circular region $S$ with radius $r_{td}$. We took cylindrical coordinates $(r, \theta, z)$ with the center $S$, as the origin. Ultrasonic waves propagate from the water to the material through the surface region $S_1$ . We consider the sound pressure of incident wave in a small region $dS_1$ as $dp_1$, the small region on the transducer as $dS$ and the distance from $dS$ to $dS_1$ as $R$. Then, $dp_1$ is given as[7],

$$dp_1 = i\omega\rho_w \frac{V_0}{2\pi} \int_0^{2\pi} \int_0^{r_{td}} \frac{e^{-ikwR}}{R} r dr d\theta \qquad (1)$$

where $i=\sqrt{-1}$, $\omega$ is angular frequency, $\rho_w$ is density of water, $k_w$ is wave number of a longitudinal wave in water and $V_0$ is a parameter representing sound pressure in water. The total sound pressure in the incident region is given as,

$$P = dp_1 dS_1 = dp_1 dx' dy' \qquad (2)$$

where the center of $S_1$ represents the origin of Cartesian coordinates $(x', y', z')$ and cylindrical coordinates $(r', \theta', z')$, simultaneously. For the inclined incident wave, the incident region $S_1$ became elliptical with radii of 1.39 mm and 1.2 mm respectively. To analyze the propagation of incident waves along the specimen surface, we applied Lamb's solution[8]. Lamb's solution provides stress and displacement solutions for the problem of harmonic change of concentrated load of $P$ on the surface of a half infinite medium. Using these solutions, the intensity of a reflected wave due to the cracks was approximately calculated. The intensity of an incident wave on crack surface was approximately calculated by integrating Lamb's solution along $S_1$. Therefore, each stress component at the crack surface is given as,

$$\sigma_{ij}(z', r') = \int_{S_1} f_{ij}(z', r') dS_1 \qquad (3)$$

here, $\sigma_{ij}(z', r')$ is each stress component of the incident wave, $f_{ij}(z', r')$ is each stress component $\bar{\sigma}_{z'r'}$, $\bar{\sigma}_{z'z'}$, $\bar{\sigma}_{r'r'}$, $\bar{\sigma}_{\theta'\theta'}$ from Lamb's solution, as defined in Eq. (4).

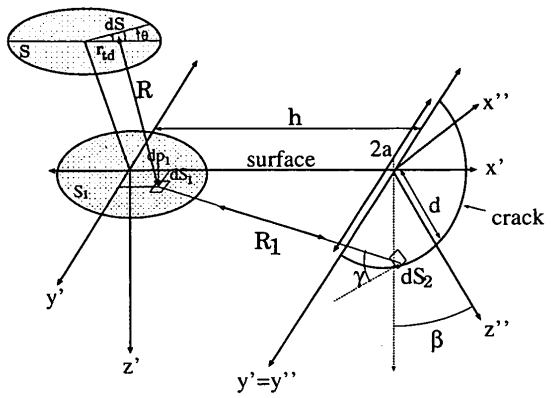


Fig. 4 Schematic for interaction of an incident wave with surface crack

$$\bar{\sigma}_{z'r'} = \frac{idp_1}{2} xN_1J_1(xr') + \frac{dp_1}{\pi} \int_0^{k_\alpha} \left\{ \frac{k^2 w(2k^2 - k_\beta^2)(e^{-wz'} - e^{-w'z'})}{F(k)} \right\} D_1(kr')dk$$
$$+ \frac{dp_1}{\pi} \int_{k_\alpha}^{k_\beta} \left\{ \frac{4k^4 w^2 w'(2k^2 - k_\beta^2)(e^{-wz'} - e^{-w'z'})}{F(k)f(k)} \right\} D_1(kr')dk$$
$$+ \frac{2dp_1}{\pi^2} \int_0^{\infty} \int_0^{\infty} \left\{ \frac{\eta^3 \sqrt{k_\alpha^2 - \eta^2}(2\eta^2 - k_\beta^2)(e^{-wz'} - e^{-w'z'})}{F(\eta)} \right\} e^{-\eta r' \cosh u} du d\eta$$

$$\bar{\sigma}_{z'z'}=\frac{idp_1}{2}xN_1J_1(xr')+\frac{dp_1}{\pi}\int_0^{k_\alpha}\left\{\frac{k^2w(2k^2-k_\beta^2)(e^{-wz'}-e^{-w'z'})}{F(k)}\right\}D_1(kr')dk$$

$$\bar{\sigma}_{r'r'}=-\frac{idp_1}{2}xN_2J_0(xr')-\frac{dp_1}{r'}xM_2K_1(xr')$$
$$-\frac{idp_1}{\pi}\int_{k_\alpha}^{k_\beta}\left\{\frac{-(2k^2-k_\alpha^2)(2k^2-k_\beta^2)2k^3ww'e^{-wz'}+(2k^2-k_\beta^2)^2k^3ww'e^{-w'z'}}{F(k)f(k)}\right\}D_0(kr')dk \quad (4)$$
$$-\frac{dp_1}{\pi r'}\int_{k_\alpha}^{k_\beta}\left\{\frac{(2k^2-k_\beta^2)8k^4ww'e^{-wz'}-(2k^2-k_\beta^2)^2k^2ww'e^{-wz'}}{F(k)f(k)}\right\}D_1(kr')dk$$

$$\bar{\sigma}_{\theta'\theta'}=\frac{idp_1}{2}xN_3J_0(xr')+\frac{idp_1}{2\pi}\int_{k_\alpha}^{k_\beta}\left\{\frac{k_\alpha^2(2k^2-k_\beta^2)^3e^{-wz'}}{f(k)}\right\}D_0(kr')dk-\frac{dp_1}{r'}xM_3K_1(xr')$$
$$-\frac{dp_1}{\pi r'}\int_{k_\alpha}^{k_\beta}\left\{\frac{-(2k^2-k_\beta^2)4k^4ww'e^{-wz'}+(2k^2-k_\beta^2)^2k^2ww'e^{-w'z'}}{F(k)f(k)}\right\}D_1(kr')dk$$

$N_1$, $N_2$, $N_3$, $M_1$, $M_2$ and $M_3$, in Eq.(4), are given as,

$$N_1=\frac{2xw_1(2x^2-k_\beta^2)(e^{-wz'}-e^{-w'z'})}{F'(x)}$$
$$M_1=\frac{(2x^2-k_\beta^2)^2e^{-wz'}-4x^2w_1w_1'e^{-w'z'}}{F'(x)}$$
$$N_2=\frac{-(2x^2-k_\alpha^2)(2x^2-k_\beta^2)e^{-wz'}+2x^2w_1w_1'e^{-w'z'}}{F'(x)}$$
$$M_2=\frac{(2x^2-k_\beta^2)xe^{-wz'}-2xw_1w_1'e^{-w'z'}}{F'(x)}$$
$$N_3=\frac{-(2x^2-k_\beta^2)xe^{-wz'}+2xw_1w_1'e^{-w'z'}}{F'(x)} \quad (5)$$
$$M_3=\frac{k_\alpha^2(2x^2-k_\beta^2)e^{-wz'}}{F'(x)}$$
$$F(k)=(2k^2-k_\beta^2)^2-4k^2ww'$$
$$f(k)=(2k^2-k_\beta^2)^2+4k^2ww'$$
$$w_2=k^2-k_\alpha^2,\quad w'^2=k^2-k_\beta^2$$
$$w_1^2=x^2-k_\alpha^2,\quad w_1'^2=x^2-k_\beta^2$$
$$D_0(kr')=K_0(kr')-iJ_0(kr')$$
$$D_1(kr')=K_1(kr')-iJ_1(kr')$$

respectively. Where, $k_\alpha$ and $k_\beta$ are wave numbers of longitudinal and transverse waves in the material, respectively. $x$ is the value of $k$ when $F(k)=0$, $J_n(kr')$ and $K_n(kr')$ are the first and second kind of order $n$ ($n=0, 1$) Bessel functions, respectively.

Consider that the angle between crack depth and $z'$ axis is $\beta$. Then, we introduce the new Cartesian coordinates ($x''$, $y''$, $z''$) for which the $y''$-$z''$ plane is on the crack surface. The crack surface was divided into small regions, and it was assumed that the small region $dy''dz''$ is the source of reflection. Here, the center of the coordinate system was expressed as ($y''$, $z''$). To calculate reflected waves from cracks, we made the following assumption. (1) The intensity of a reflected wave is inversely proportional to the distance from the reflection point to reception point $R+R_1$. (2) The intensity of a reflected wave is proportional to the intensity of the incident wave. (3) An incident surface wave propagates in the same direction as the inclination incidence angle in water. Then, the reflected wave from the cracks is given as

$$d\sigma_{ij}^R(y'', z'')=\int_{S_1}\sigma_{ij}C\frac{2r_{td}}{R+R_1}\cos(\gamma)dx'dy' \quad (6)$$

Here, $C$ is the reflection rate, $r_{td}$ is the radius of the transducer, $R_1$ and $\gamma$ are represented as

$$\left.\begin{aligned}R_1&=\sqrt{h''^2+(z''\cos\beta)^2}\\ \gamma&=\tan^{-1}\frac{z''\cos\beta}{h''}+\beta\\ h''&=\sqrt{(y'-y'')^2+(h-x'+z''\sin\beta)^2}\end{aligned}\right\} \quad (7)$$

Furthermore, the reflection occurred on all crack surfaces, so the above equation must be integrated along $S_2$.

$$\sigma_{ij}^R=\int_{S_2}\int_{S_1}\sigma_{ij}C\frac{2r_{td}}{R+R_1}\cos(\gamma)dx'dy'dy''dz'' \quad (8)$$

## 4. Experiment Results and Discussion

### 4.1 Surface observation results

Load repetition caused many slip bands to be generated. Furthermore, increase in the number of cycles was accompanied by the transition from slip bands to small fatigue cracks. Subsequently, the numerous small fatigue cracks propagate, coalescence and become macroscopic cracks. Figure 5 shows sample photographs of the surface and cross-sectional view of observed cracks of 175 μm length. The crack is 60 μm in depth and nearly perpendicular to the surface. This crack is labeled crack No. 5. The measurement results of surface length and depth of the cracks are shown in Table 3.

### 4.2 Ultrasonic evaluation results

Figure 6 shows a typical reflected wave from the cracks shown in Fig. 5. The inclined incidence wave had a distributed arrival time, thus the reflected wave has a wide spread along the time axis. In addition to the reflected wave due to the cracks (shown as A in Fig. 6), forest echoes of the reflected wave due to grain boundaries are also observed. This kind of echo was considered to affect the sensitivity of the crack detection procedure[9].

Figure 7 shows the change of maximum value of maximum amplitude of reflected wave, $A_{max}$, due to the increase of the number of cycles, for crack No. 5. The relationship between crack length and number of cycles is also shown. Here, Amax was normalized by Aedge (maximum value of maximum amplitude of reflected wave from specimen edge). This crack was arrested at $N=138\,000$ and was 175 μm in length. Up

Table 3 Crack length, depth and deflection angle

| No | 2a[μm] | d[μm] | d/a | β[degree] |
|---|---|---|---|---|
| 1 | 50 | - | - | - |
| 2 | 70 | 26 | 0.743 | 0 |
| 3 | 115 | 40 | 0.696 | 0 |
| 4 | 150 | 50 | 0.667 | 0 |
| 5 | 175 | 60 | 0.686 | 0 |
| 6 | 215 | 90 | 0.837 | 10 |
| 7 | 580 | 240 | 0.828 | 20 |

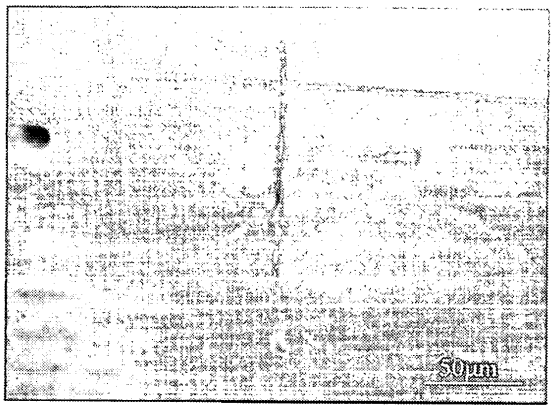


(a) Surface view

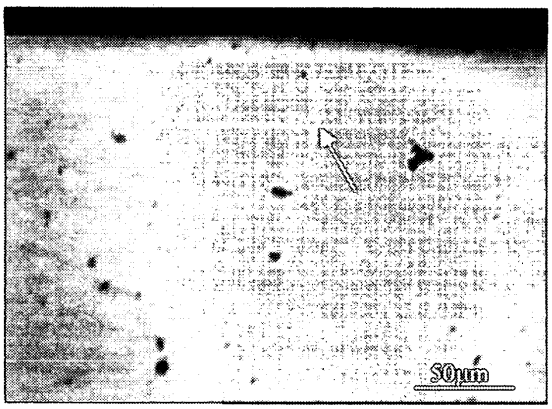


(b) Cross-sectional view

Fig. 5 Photo of small surface crack (crack length 175 μm)

to 100 000 cycles, the crack propagated by 10 μm, and the corresponding maximum amplitude of the reflected wave shown no significant change. At $N=$ 138 000 the crack propagated abruptly, and simultaneously, the maximum amplitude of the reflected wave increased significantly.

In the following, we present measurement results for seven arrested fatigue surface cracks at $N=$ 138 000. Figure 8 shows the relationship between maximum amplitude of reflected wave, $A_{max}/A_{edge}$, and surface crack length, $2a$. Symbols represent experimental results and the line represents simula-

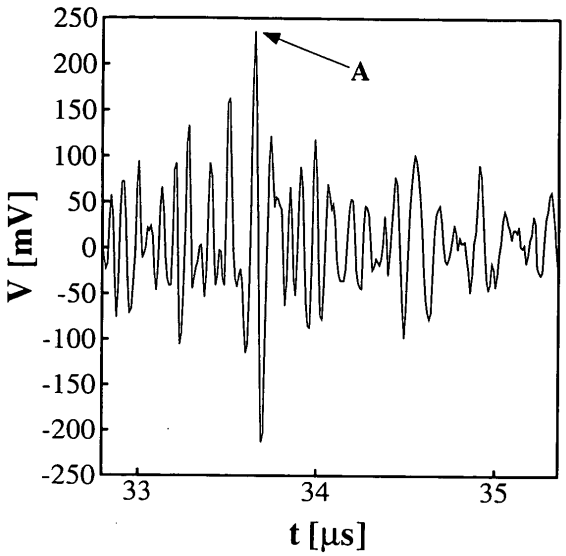


Fig. 6 Waveform of reflected wave by 175 μm-long surface crack

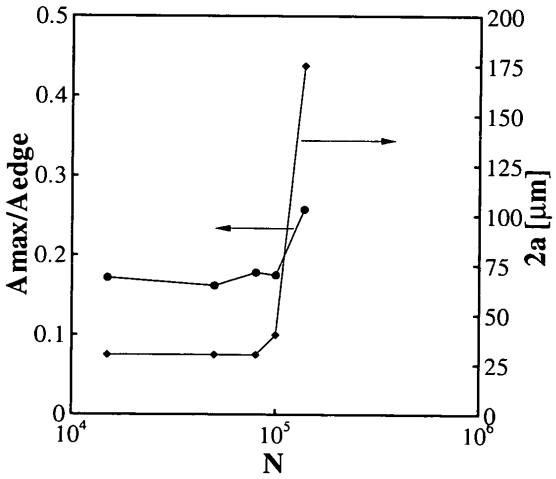


Fig. 7 Relationship between maximum amplitude and number of cycles

tion results from Lamb's solution. Simulation results here were obtained using $\sigma_{z'z'}$ in Eq.(8) and the constant of $V_0 \cdot C$ was determined from the experimental result of crack length $2a=215$ μm ($\phi=-30°$). Solid and open symbols represent results for incidence angles of $\phi=30°$ and $\phi=-30°$, respectively. The error bars indicate the fluctuation of amplitude acquired. From this figure it can be seen that increases in the crack lengths are associated with increase of $A_{max}/A_{edge}$. It is considered that the longer crack lengths have a wider crack surface area which in results in that more ultrasonic waves are reflected. The ultrasonic evaluation result at the initial condition showed $A_{max}/A_{edge}$ of 0.19, while the cracks of 50 and 70 μm length result in the same level of $A_{max}/A_{edge}$. These results showed that in this measurement condition (stainless steel, fine polished

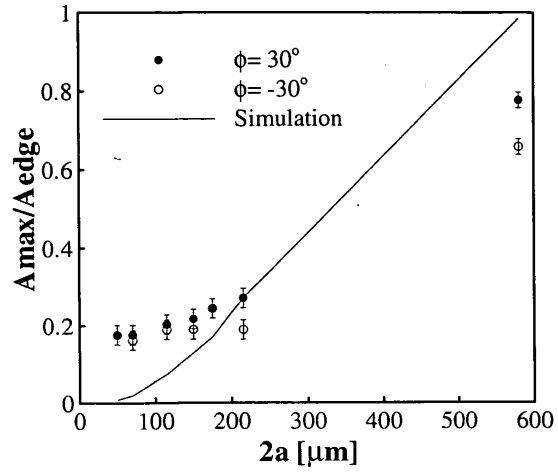


Fig. 8 Relationship between maximum amplitude and crack length

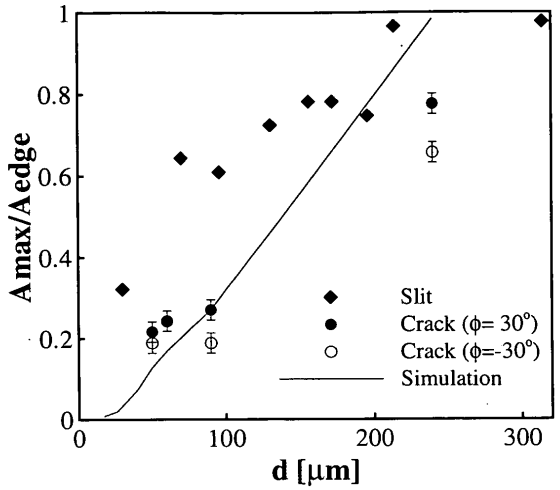


Fig. 9 Relationship between maximum amplitude of reflected wave and crack depth

surface, 10 MHz frequency) it is difficult to evaluate cracks less than 70 μm in length. The average diameter of grain boundary of this specimen is about 40 μm. Because this dimension is close to the crack length, 50 and 70 μm, it is difficult to identify whether the reflected wave is from the cracks or grain boundaries. For the cracks 115 μm or more in length, the intensity of reflected waves increased significantly, and thus, they can be distinguished from the waves reflected at the grain boundaries.

For 215 and 580 μm long cracks, a difference in $A_{max}/A_{edge}$ occurred when the incidence angle changed. From the cross-sectional observation, it is seen that these cracks were inclined at 10 and 20 degrees, respectively. The direction of this inclination is that yielding a larger $A_{max}/A_{edge}$ value. Consequently, this result reveals that the change of incidence angle yields an important information on the crack inclination.

Figure 9 shows the relationship between $A_{max}/A_{edge}$ and crack depth, $d$. Circles and diamonds represent fatigue cracks and artificial notches, respectively. The solid and open symbols represent incidence angle of 30 degrees and −30 degrees, respectively. The line represents simulation results obtained using Lamb's solution. For both fatigue cracks and artificial notches, the increase of cracks depth caused the increase of $A_{max}/A_{edge}$. The increase of $A_{max}/A_{edge}$ saturates over the depth of 200 μm. Because the incidence waves to the crack are surface waves, they penetrate within one wavelength in depth while propagating. Therefore, the crack depth in the wavelength of the incident wave will give the maximum value of reflected intensity, for cracks depth greater than the wavelength, there is no more effect on reflected intensity. The ultrasonic surface wave used in this study (10 MHz) has a 280 μm wavelength. Comparing the results of fatigue cracks and artificial notches, for the same depth, artificial notch results show a higher value of $A_{max}/A_{edge}$. Even at the same depth, artificial notches have a wider surface area compared to the fatigue cracks. Furthermore, it can be considered that in the case of fatigue cracks, there was crack closure. Compared to the large cracks, small cracks have large crack opening ratios. Therefore, we treated the relationship between ultrasonic wave parameters and "crack length, and crack depth", by including the influence of crack closure.

From Figs. 8 and 9, it is clear, under these conditions (stainless steel, fine polished surface, 10 MHz frequency), the use of the ultrasonic immersion method could enable detection of small fatigue cracks larger than 115 μm in length and 40 μm in depth.

Figure 10 shows the relationship between maximum amplitude of reflected wave, $A$, and incidence wave position, $h$. Symbols and lines represent experimental and simulation results, respectively. In the vertical axis, $A$ was normalized as $(A-A_{min})/(A_{max}-A_{min})$, where $A_{min}$ is the value of $A$ at $h=-1\,800$ μm. Simulations were conducted using crack shape ratio $d/a$ shown in Table 3, and crack deflection $\beta$ was assumed equal to zero. Increasing of the distance from the crack to incident points caused $(A-A_{min})/(A_{max}-A_{min})$ to decrease. For $h<0$ $(A-A_{min})/(A_{max}-A_{min})$ decreased gradually, on the other hand for $h>0$ $(A-A_{min})/(A_{max}-A_{min})$ decreased rapidly. When ultrasonic waves are incident in front of the defect, surface waves will propagate toward the crack and will be reflected by the crack, so the ultrasonic intensity gradually decreases. In other words, the affected parameter was the propagation path. On the other hand, when ultrasonic waves incident at a point beyond the crack, surface waves will propagate with-

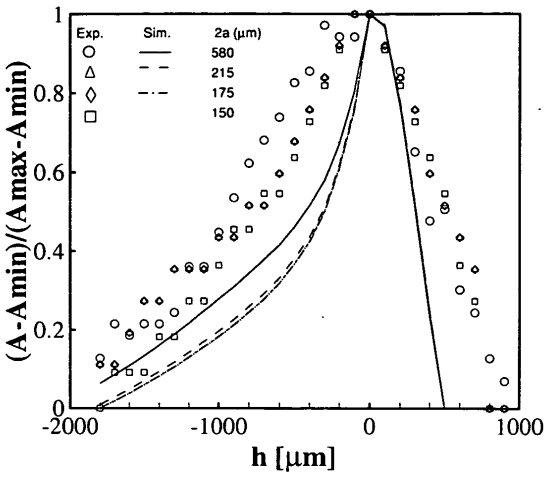


Fig. 10 Relationship between reflected wave amplitude and distance from incidence point to surface fatigue cracks

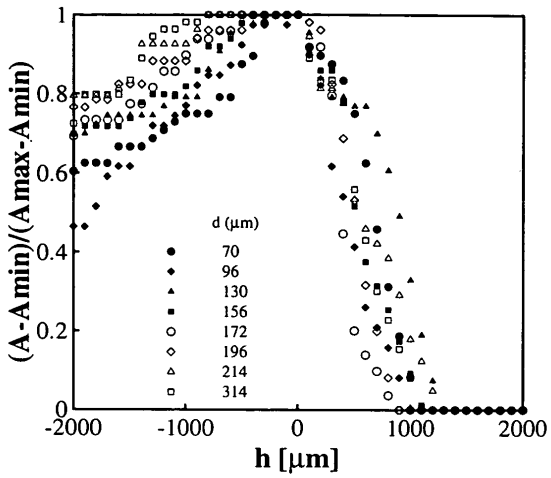


Fig. 11 Relationship between reflected wave amplitude and distance from incidence point to artificial defects

out any obstacle. This did not cause any reflected surface waves. So, the ultrasonic intensity decreased significantly. Comparing the experimental and simulation results, along $h<0$, it is seen that they coincide with each other in the case of $(A-A_{min})/(A_{max}-A_{min})$ increasing with the increase of crack lengths.

Figure 11 shows the relationship between maximum amplitude of reflected wave $A$ and incident wave position $h$ for the artificial notches. This figure shows the same tendency as seen in Fig. 10.

Figure 12 shows the relationship between $(A-A_{min})/(A_{max}-A_{min})$ and defect depth, $d$, at $h=-500$, $-1\,000$ and $-1\,500$ μm. Solid and opened symbols represent experimental results on artificial notches and on fatigue cracks, and lines (solid, dashed, dashed and dotted) represent the simulation results. As shown in Fig. 9 (at $h=0$), which shows that the maximum amplitude of the reflected wave increases with the increase in crack depth, Fig. 12 shows the same phenomenon in according to the increase of crack depth. Both artificial notches and fatigue cracks slopes show the same level of steepness.

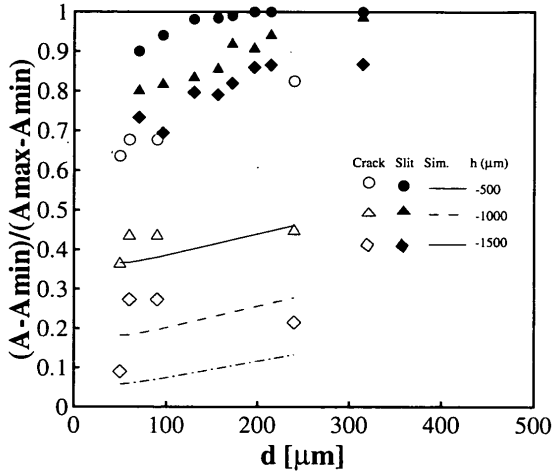


Fig. 12 Relationship between reflected wave amplitude and defect depth

### 4.3 Internal geometry evaluation of surface cracks

To confirm the crack length and depth dependence of the ultrasonic wave parameter (both $A_{max}/A_{edge}$ and $(A-A_{min})/(A_{max}-A_{min})$), the following simulations (model shown in Fig. 13) have been carried out. (1) Changing crack depth under fixed crack length (base on the cracks with 215 μm length and 50 μm depth), (2) Changing crack length under fixed crack depth (base on the cracks with 70 μm length and 90 μm depth).

Figures 14 and 15 show the relationship between the change of $(A_{max}/A_{edge})$, $(A-A_{min})/(A_{max}-A_{min})$ and increase of crack depth ($\Delta d$) and of increase of crack length ($\Delta 2a$), respectively. The lines in the figures represent values obtained by the least squares method. Comparing the slopes in Figs. 14 and 15, the slope for $\Delta d$ is seen to be larger. This means that the dependency of $(A_{max}/A_{edge})$ and $(A-A_{min})/(A_{max}-A_{min})$ on the crack depth is more than that on the crack length.

Through the difference of the dependency above, using $(A_{max}/A_{edge})$, $(A-A_{min})/(A_{max}-A_{min})$ the experimental equations of the linear relation to calculate both crack depth and crack length are proposed as,

$$2a=c_{11}\frac{A_{max}}{A_{edge}}+c_{12}\frac{A-A_{min}}{A_{max}-A_{min}}+c_{13}$$
$$d=c_{21}\frac{A_{max}}{A_{edge}}+c_{22}\frac{A-A_{min}}{A_{max}-A_{min}}+c_{23} \quad (9)$$

Using the experimental results of known inner geometry, $(A_{max}/A_{edge})$ and $(A-A_{min})/(A_{max}-A_{min})$, the least squares method approximation was carried out to determine the coefficients, and the results are as

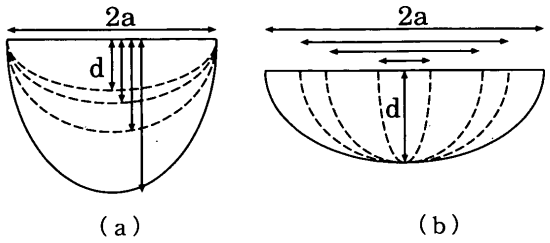


Fig. 13 Crack geometry used in simulation to clarify crack depth and length dependence of reflected wave amplitude

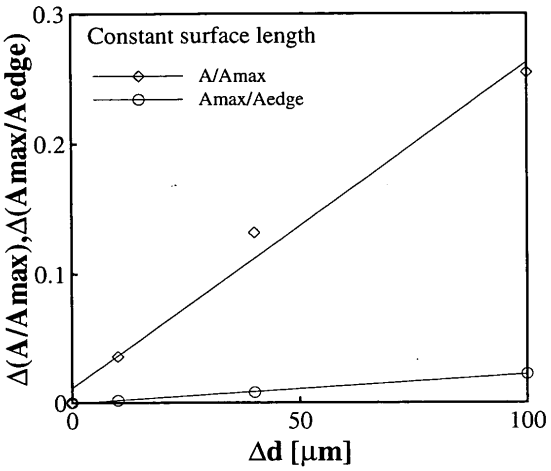


Fig. 14 Relationship between change of defects and change of ultrasonic parameters

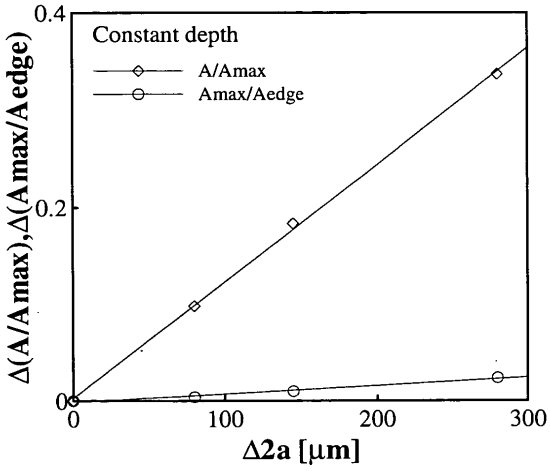


Fig. 15 Relationship between change of defects and change of ultrasonic parameters

follows:

$c_{11}=1.17\times10^{3}$; $c_{12}=1.16\times10^{2}$; $c_{13}=-1.78\times10^{2}$

$c_{21}=5.15\times10^{2}$; $c_{22}=2.89\times10^{1}$; $c_{23}=-7.68\times10^{1}$

The above equations are valid in the range of $2a=70\sim215$ μm and $d=40\sim90$ μm. Figure 16 shows the relationship between crack depth, crack length and $A_{max}/A_{edge}$. Figure 17 shows the relationship between crack depth, crack length and $(A-A_{min})/A_{max}-A_{min})$.

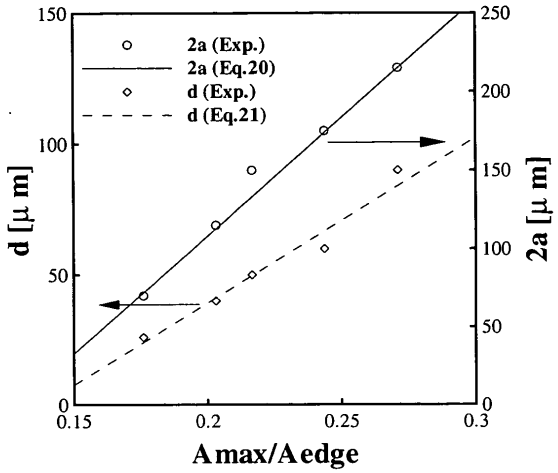


Fig. 16 Relationship between $A_{max}/A_{edge}$ and defect depth or length

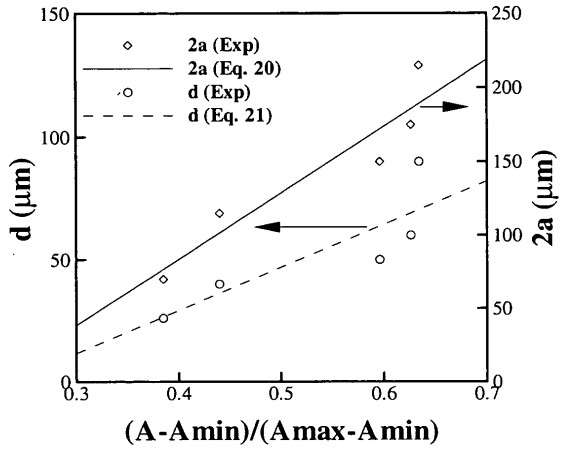


Fig. 17 Relationship between $(A-A_{min})/(A_{max}-A_{min})$ and defect depth or length

Circles and diamonds represent measurement results of crack depth and crack length, respectively, while solid lines represent the linear approximation of the calculation result from Eq.(9). The calculation results coincide with experimental results within a 10% error margin. Thus, for the conditions used in this study (stainless steel, fine polish surface, 10 MHz frequency), Eq.(9) is valid to evaluate crack depth and crack length.

## 5. Conclusions

With the aim of investigating the validity of the ultrasonic water immersion method with oblique incidence to evaluate low-cycle fatigue damage non-destructively, we proposed a method to evaluate depth and deflection of small surface fatigue cracks using the change of maximum amplitude of reflected waves due to the change of the distance between the incidence point and cracks. The obtained results are summarized as follows:

1. Using the water immersion ultrasonic method with large incidence angle of the 10 MHz center frequency, surface crack length and crack depth of the fatigue crack can be evaluated non-destructively using the maximum amplitude ($A_{max}/A_{edge}$ and $A/A_{max}$) of the reflected surface wave. Under the conditions used in this experiment, cracks of 115 μm length and 50 μm depth and larger can be evaluated.

2. Using two parameters of $A/A_{max}$ and $A_{max}/A_{edge}$, an empirical formula to calculate surface crack length, $2a$, and crack depth, $d$, was proposed. This equation is valid within $2a=70$ μm$\sim$215 μm, $d=$ 26 μm$\sim$ 90 μm with a 10% error margin.

3. Though the gradient along the depth direction of the crack is detectable qualitatively, further examination is necessary to estimate it quantitatively.

## References


(1) Forsyth, P.J.E., The Physical Basis of Metal Fatigue, (1969), pp. 34-72, Blackie and Son Ltd.

(2) Saka, M. and Takanaka, Y., Inverse Analysis of Closed Crack Ultrasonic Inspection, Trans. Jpn. Soc. Mech. Eng., (in Japanese), Vol. 56, No. 528, A (1990), pp. 1736-1742.

(3) Ahmed, S.R. and Saka, M., A Sensitive Ultrasonic Approach to NDE of Tightly Closed Small Cracks, Transaction of the ASME, Vol. 120 (1998), pp. 384-392.

(4) Yamanaka, K. and Enomoto, Y., Observation of Surface Cracks with Scanning Acoustic Microscope, J. Appl. Phys., Vol. 53, No. 2 (1982), p. 846.

(5) Hirao, M., et al., Small Fatigue Crack Behavior in 7075-T651 Aluminum as Monitored with Rayleigh Wave Reflection, Metallurgical Transactions A, Vol. 24A (1993), pp. 1773-1783.

(6) Cyril, S.S. and Lester, G., Measurement of Internal Boundaries in Three-Dimensional Structures By Random Sectioning, Journal of Metals, (1953), pp. 81-87.

(7) Sirado, K., Acoustics Engineering, Soc. Electrocommunication, (1984), pp. 49-60, Corona Publishing Co. Ltd.

(8) Lamb, H., On the Propagation of Tremors Over the Surface of an Elastic Solid, Phil. Trans. Roy. Soc. (London) A, Vol. 203 (1904), pp. 1-42.

(9) Worlton, D.C., Ultrasonic Testing with Lamb Waves, Nondestructive Testing, (1957), pp. 218-222.